Research article

Overstretching alveolar epithelial type II cells decreases surfactant secretion via actin polymerization and intracellular trafficking alteration

Shigesato Inoue [a,b,*], Junpei Nagao [b], Kouhei Kawamoto [b], Keiko Kan-o [a], Satoru Fukuyama [a,c], Saori Sasaki [d], Susumu Kudo [d], Isamu Okamoto [a], Toshihiro Sera [d,e]

[a] Department of Respiratory Medicine, Graduate School of Medical Sciences, Kyushu University, Fukuoka, Japan
[b] Department of Mechanical Engineering, Graduate School of Engineering, Kyushu University, Fukuoka, Japan
[c] Department of Respiratory Medicine, National Hospital Organization Omuta National Hospital, Fukuoka, Japan
[d] Department of Mechanical Engineering, Faculty of Engineering, Kyushu University, Fukuoka, Japan
[e] Department of Medical and Robotic Engineering Design, Faculty of Advanced Engineering, Tokyo University of Science, Tokyo, Japan

ARTICLE INFO

ABSTRACT

Pulmonary surfactant is essential for maintaining proper lung function. Alveolar epithelial type II (AE2) cells secrete surfactants via lamellar bodies (LBs). In tidal loading during each breath, the physiological cyclic stretching of AE2 cells promotes surfactant secretion. Excessive stretching inhibits surfactant secretion, which is considered to contribute to the development of lung damage. However, its precise mechanism remains unknown. This study tested whether actin polymerization and intracellular transport are required for pulmonary surfactant secretion and the association of actin polymerization and transport in identical human AE2-derived A549 cells using live-cell imaging, not in the bulk cells population. We found that overstretching approximately doubled actin polymerization into filaments (F-actin) and suppressed LB secretion by half in the fluorescent area ratio, compared with physiological stretching (F-actin: 1.495 vs 0.643 (P < 0.01); LB: 0.739 vs 0.332 (P < 0.01)). An inhibitor of actin polymerization increased LB secretion. Intracellular tracking using fluorescent particles revealed that cyclic stretching shifted the particle motion perpendicularly to the direction of stretching according to the orientation of the F-actin (proportion of perpendicular axis motion prior particle: 0h 40.12 % vs 2h 63.13 % (P < 0.01)), and particle motion was restricted over time in the cells subjected to overstretching, indicating that overstretching regulates intracellular transport dynamics (proportion of stop motion particle: 0h 1.01 % vs 2h 11.04 % (P < 0.01)). These findings suggest that overstretching changes secretion through the cytoskeleton: overstretching AE2 cells inhibits pulmonary surfactant secretion, at least through accelerating actin polymerization and decreasing intracellular trafficking, and the change in actin orientation would modulate intracellular trafficking.

---

* Corresponding author. Department of Respiratory Medicine, Graduate School of Medical Sciences, Kyushu University, 3-1-1 Maidashi, Higashi-ku, Fukuoka, 812-8582, Japan.
E-mail address: shigesato_inoue@kyudai.jp (S. Inoue).

1. Introduction

Pulmonary surfactants, a complex mixture of phospholipoproteins, line the air–liquid interface and reduce surface tension, contributing to alveolar stability [1]. The alveolar epithelium is a mixed monolayer consisting of alveolar epithelial type I (AE1) and II (AE2) cells, which are responsible for gas exchange and synthesis and for the secretion of pulmonary surfactants, respectively [2–4]. In AE2 cells, pulmonary surfactants are stored in characteristic organelles called lamellar bodies (LBs) [5]. Physical stimuli, such as mechanical stretching, are involved in the secretion process from AE2 cells [2,6,7], depending on the stretch intensity and pattern. A large tidal volume depletes the surfactant secretion, which is considered to contribute to the development of lung damage known as ventilator-induced lung injury [8]. The secretion was increased by cyclic physiological stretching, while it decreased by overstretching [9].

Cytoskeletal components, particularly the actin cytoskeleton, are also considered to play a crucial role in LB secretion [10–14]. Actin is polymerized or depolymerized by chemical [15] and physical stimuli [16]. Actin fiber stabilization by jasplakinolide, an actin-polymerizing peptide, inhibits β-agonist-induced surfactant secretion from AE2 cells [13]. Actin depolymerization by the botulinum C2 toxin increases the secretion from AE2 cells, and actin stabilization by phalloidin prevented this C2 toxin–specific increase in secretion, suggesting that surfactant secretion from AE2 cells may be enhanced by actin depolymerization and inhibited by actin stabilization [14]. Regarding physical stimuli, high shear stress decreases LB secretion from AE2-derived A549 cells, exhibiting fragmented and disorganized actin (F-actin) [17]. Moreover, a previous study using quantum dots introduced to cells found that drug-promoted actin depolymerization resulted in a higher diffusion coefficient and larger confinement size of fluctuations [18]. In these previous studies, F-actin was stained with phalloidin after fixation, and the amount of surfactant secretion was evaluated as the percentage of [^{3}H]phosphatidylcholine in the medium corrected by the total amount in the cells and medium. Therefore, it is not clear that the changes in secretion and actin polymerization over time are due to mechanical stretching of the identical living cells, not changes of the bulk cells population.

Here, we hypothesized that actin polymerization by invasive mechanical stretching would inhibit intracellular trafficking and affect the secretory mechanism in AE2 cells, resulting in decreased surfactant release. We first compared the relationship among the stretch amplitude of identical cells, actin polymerization, and surfactant secretion based on live imaging of human AE2-derived A549 cells by tracking the same cells over time. LB area reduction in the same AE2 cells was defined as the ability to secrete surfactant and polymerize actin, and LBs and F-actin in AE2 cells were stained simultaneously with quinacrine [17,19,20] and silicon rhodamine (SiR) [21], respectively; then their redistributions after cyclic stretching for several hours were measured using confocal microscopy. There have been no studies that have quantitatively evaluated changes in stretch conditions, cellular changes, and intracellular trafficking. In addition, to characterize the changes in intracellular trafficking caused by mechanical stretching, we delivered and tracked the fluorescence particles in AE2 cells to quantitatively evaluate the intracellular trafficking by analyzing the mean squared displacement (MSD).

2. Materials and methods

2.1. Cell culture

A549 cells (RRID: JCRB0076) were obtained from Japanese Collection of Research Bioresources Cell Bank in Japan. They were cultured in Dulbecco's Modified Eagle's Medium (DMEM) (GIBCO, Thermo Fisher Scientific, USA) containing 10 % fetal bovine serum (Thermo Fisher Scientific) and 1 % antibiotic-antimycotic (10,000 units/mL penicillin, 10,000 μg/mL streptomycin, and 25 μg/mL Amphotericin B, Thermo Fisher Scientific) in humidified incubators containing a 5 % CO_2 atmosphere at 37 °C.

2.2. Stretch chamber and stretching device

The custom-made stretch chambers were made of KE-106 silicone (Shin-Etsu Chemical Co., Japan). Briefly, a silicone elastomer base and curing agent mixture were poured into a mold and baked for 1 h at 150 °C. The molded flexible silicone block that constituted our stretch chamber had a 10 mm square with a 0.1 mm thick silicone membrane in the center where cells could be seeded. The square bottom was coated with 50 μg/mL fibronectin (Sigma-Aldrich Corp., USA) diluted in phosphate-buffered saline (PBS) to facilitate cell attachment to the silicone surface. For the experiments, the chamber was attached to a custom-made conventional stretching device mounted on a confocal microscope stage (A1R, Nikon Corp., Japan). Computer-controlled stepping motors (AZM24AK, Oriental Motor, Japan) applied uniaxial and horizontal distension to the silicon chamber. Under the stretch protocol, cells were subjected to 0, 10, and 20 % strains at a rate of 15 cycles/min for 0, 1, and 2 h. In this study, 10 and 20 % strains were assumed to be normal and to cause high deformation in the cells [22], which we considered physiological and invasive and which is equivalent to a 21 % 44 % area change (equivalent to 1.1 and 1.2 squared), respectively. The temperature was maintained at a constant 37 °C by warm air during the experiment.

2.3. Simultaneous live-cell imaging

Quinacrine (Wako, Japan) and SiR-actin (Cytoskeleton Inc., USA) were used to image LBs and F-actin in living AE2 cells simultaneously. Cells cultured in a stretch chamber were loaded with 200 nM SiR-actin and incubated at 37 °C in a 5 % CO_2 atmosphere for 24 h. After being washed twice with PBS, the cells were loaded with 5 μM quinacrine and incubated for 60 min. After the cells were

washed twice with HBS and subjected to the stretch stimuli described above, the redistribution of LBs and actin in the same AE2 cells was imaged at 1 μm intervals by a confocal microscope (A1R, Nikon Corp., Japan) fitted with a 60x water-immersion lens (CFI Plan Apo VC, Nikon Corp., Japan). Quinacrine was excited at 488 nm; a 510 nm dichroic mirror and a 535 ± 50 nm emission filter were used. SiR-actin was excited at 640 nm; a 660 nm dichroic mirror and a 700 ± 75 nm emission filter were used as well.

Carboxyl group–modified fluorescent polystyrene beads (100 nm; Polysciences Inc.) were used for evaluating intracellular trafficking from the mean squared displacement (MSD) [23]. DMEM containing the prepared fluorescent particles at 0.05 mg/mL was added to the cells and placed in an incubator (37 °C, 5 % CO_2) for 2 h. The supernatant solution was replaced by HBS, and the cells were observed under a fluorescence microscope. Images were acquired every 0.04 s to a total of 950 frames under a fluorescence microscope (ECLIPSE Ti2, Nikon Corp., Japan) with a 100x oil immersion lens (CFI Plan Apo chromatic lambda objective, Nikon Corp., Japan). The fluorescent particles were excited at 470 nm; a 495 nm dichroic mirror and a 525 ± 50 nm emission filter were used as well.

2.4. Image analysis and statistics

To evaluate the LB and F-actin redistributions after cyclic stretching, fluorescent images were analyzed using ImageJ software [24]. A specific region of interest (ROI) comprising a single cell was selected from each slice. The LB and F-actin areas in ROIs were measured using appropriate threshold value binarization. Finally, the LB and F-actin area changes at t = 1 and 2 h were calculated by dividing the respective areas at t = 0 h in the identical cell.
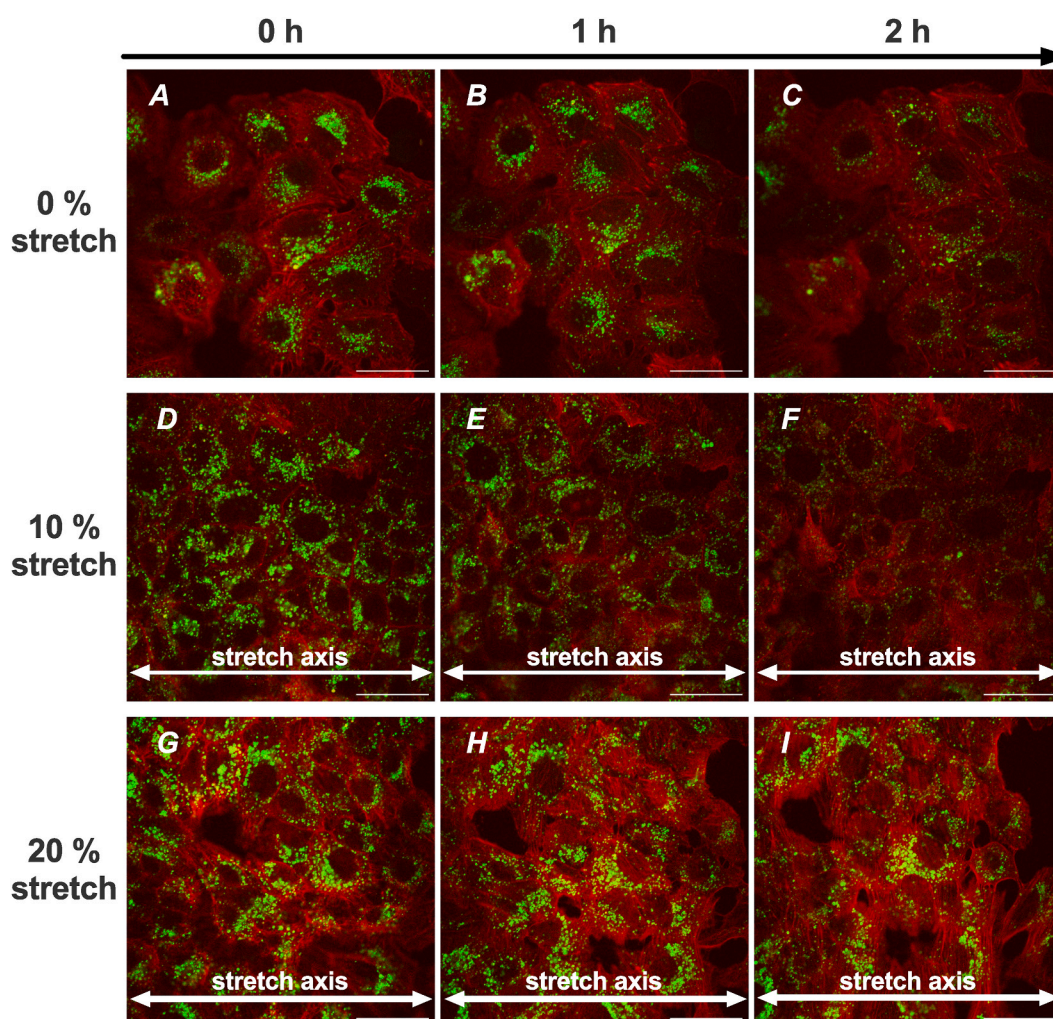
Fig. 1. Representative fluorescence images of quinacrine (green) and F-actin (red) in living AE2 cells on a silicone chamber. 0 % stretch: (A) t = 0 h, (B) t = 1 h, and (C) t = 2 h; 10 % stretch: (D) t = 0 h, (E) t = 1 h, and (F) t = 2 h; 20 % stretch: (G) t = 0 h, (H) t = 1 h, and (I) t = 2 h. (B) and (C) were captured from the same area 1 and 2 h after (A) was taken, respectively. (E) and (F) were captured 1 and 2 h after (D) was taken, respectively. (H) and (I) were captured 1 and 2 h after (G) was taken, respectively. The same areas were captured under each condition. White two-way arrows indicate the stretch axis. Scale bars are 50 μm. (For interpretation of the references to colour in this figure legend, the reader is referred to the Web version of this article.)

For tracking the fluorescent particles to calculate the MSD, the FIJI plug-in TrackMate [25] was used to track the motion of individual particles. The MSD was calculated as a function of the time lag (nΔt), with a time interval Δt (=0.04 s) and n as the number of frame intervals, using equation (1) [26–28].

$$\text{MSD}(n\Delta t) = \frac{1}{N-1-n} \sum_{i=1}^{N-1-n} \{(x(i\Delta t + n\Delta t) - x(i\Delta t)\}^2 + \{(y(i\Delta t + n\Delta t) - y(i\Delta t)\}^2 \tag{1}$$

N and i are the total number of frames and frame number, respectively. x(iΔt) and y(iΔt) are the x and y coordinates of the particle in the image at frame number i, respectively. Furthermore, to classify the particle motion, we calculated the gradient between the MSD and the time interval in both logarithms at every time interval and defined α as their average values until nΔt = 10 s α < 0.1 was considered stoppage; 0.1 < α < 0.9 was subdiffusion, 0.9 < α < 1.1 was Brownian motion; and 1.1 < α was superdiffusion [29].

2.5. Actin staining and actin direction analysis

To examine the change in F-actin orientation, the cells under each condition were fixed with 4 % paraformaldehyde soon after the stretch stimulation in a silicone chamber for 15 min and washed three times in PBS. The cells were immersed in PBS 0.1 % Triton X-100 for 15 min and immunostained with 100 μM Phalloidin-iFluor™ 647 (AAT Bioquest Inc., USA) PBS solution for 30 min while shaded from the light. After that, the cells were washed another three times in PBS, and the chamber hollow was filled with HBS for observation. Each F-actin was tracked using the ImageJ software, and the orientation was calculated before and after stretching under each condition.
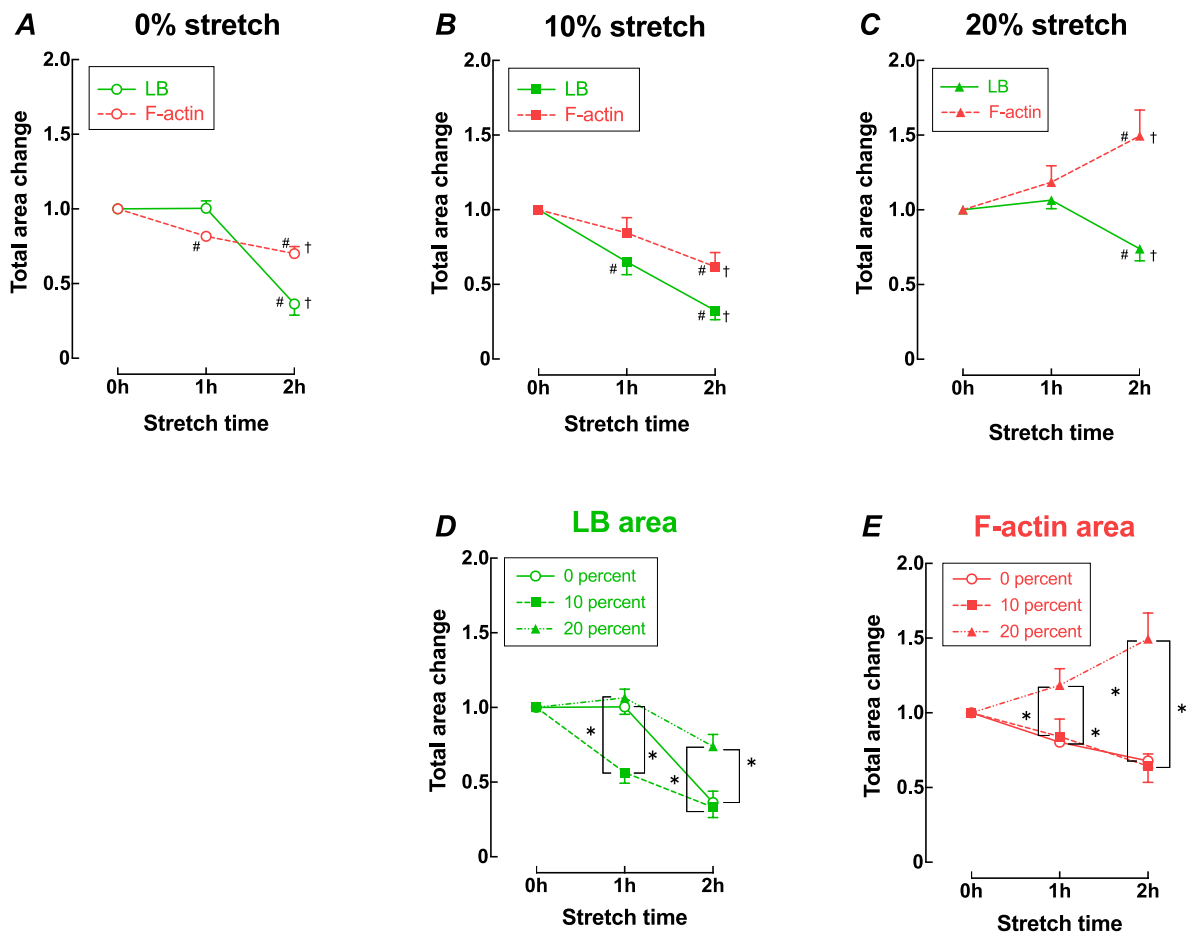
Fig. 2. **Total area change in the time course for each stretch pattern amplitude of LBs and actin in AE2 cells.** (A) 0 % stretch: N = 5, n = 18. (B) 10 % stretch: N = 5, n = 15. (C) 20 % stretch: N = 5, n = 16. The number of silicone chambers and the number of cells are denoted by N and n, respectively. The values are normalized at t = 0 h. The amount is defined as the sum in all slices. Changes in the total area of LBs (D) and of actin (E) in each cell, which are averaged for each condition, are shown over time. The values are normalized at t = 0 h. The amount is defined as the sum in all slices. Error bars indicate the standard error of the mean. *P < 0.05 (comparison between each stretch amplitude); #P < 0.05 (comparison of the 0 h time point and the 1 h or 2 h time point); †P < 0.05 (comparison of 1 h and 2 h time points).

2.6. Statistical analysis

Statistical analyses were performed using one-way repeated measures of variance (ANOVA) of the fluorescent image area on the same cell for LBs and F-actin for each time course. A one-way ANOVA was used to compare the stretch patterns. A two-way ANOVA was used for each ninth quartile point and time course of LB and F-actin distribution. We also used a one-way ANOVA to compare the time variation of α and F-actin orientation under each stretch pattern. We classified the particle motion under each stretch condition into four α classes (stoppage, subdiffusion, Brownian motion, or superdiffusion) based on the calculated value of α. We evaluated the proportion of particles in each class out of the total number of particles. Fisher's exact test was performed to assess the proportion differences within each class. The chi-squared test was used to analyze the proportion of each particle's movement classified as belonging to the value of α on the two axes (stretch axis and perpendicular axis), whichever number was larger. For multiple
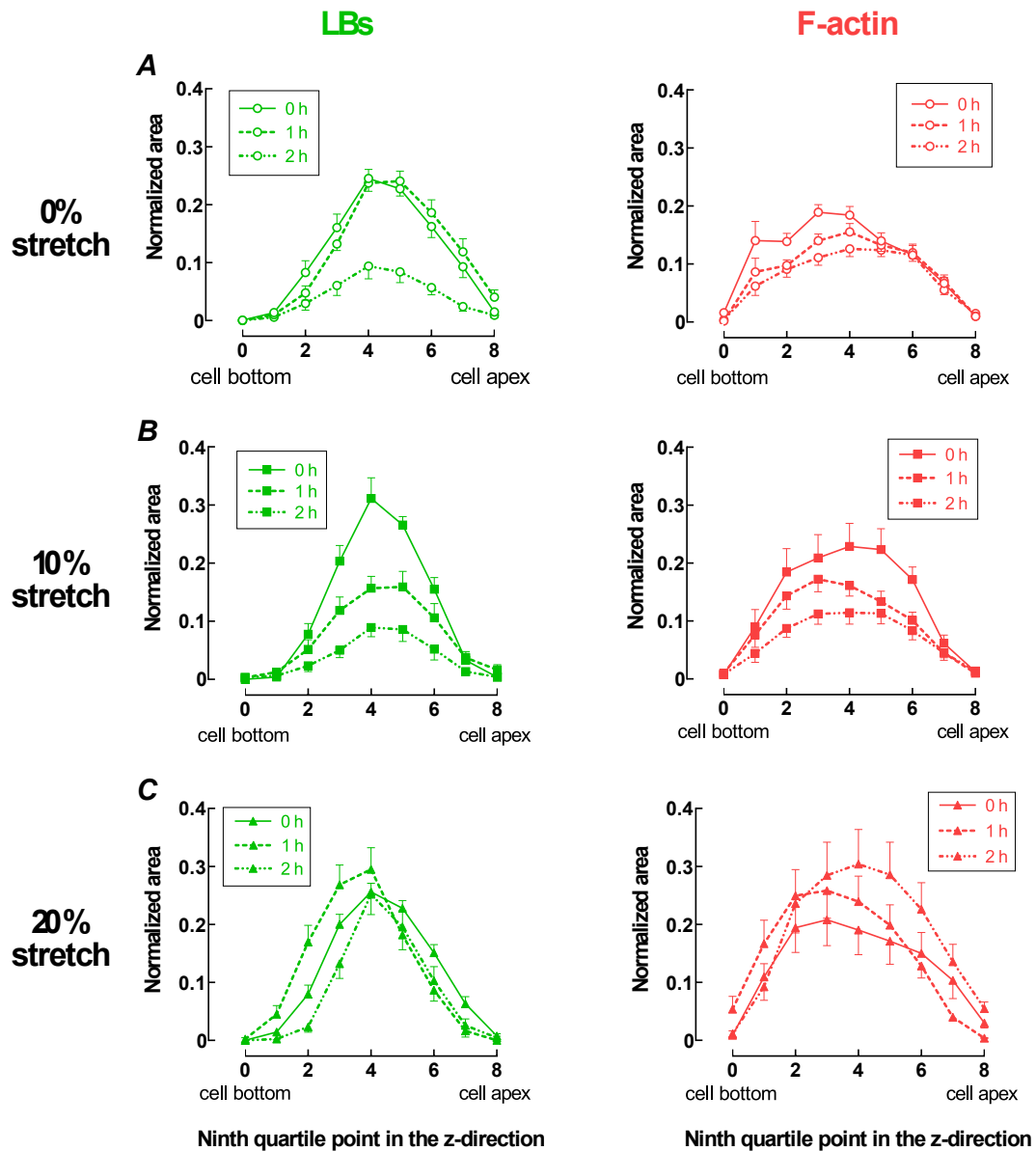
Fig. 3. The effects of each stretch pattern on LB (left side) and actin (right side) distribution. (A) 0 % stretch: N = 5, n = 18. (B) 10 % stretch: N = 5, n = 15. (C) 20 % stretch: N = 5, n = 16. The number of silicone chambers and the number of cells are denoted by N and n, respectively. Ninth quartile points are defined as follows: 0 in the figures is taken as the cell bottom, and 8 is the cell apex; the smaller the number, the closer to the bottom, and the larger the number, the closer to the top. The horizontal black lines are the mean of each data set, and the error bars indicate the standard error of the mean. All of the distributions of LBs and F-actin under each condition show significant differences over the time course (two-way ANOVA; P < 0.01).

comparisons, a one-way ANOVA was performed, followed by a post hoc Tukey test (analyzing the fluorescent image area of LBs and F-actin) or Kruskal–Wallis test (analyzing the α and F-actin orientation under each stretch condition). The Fisher's exact test and chi-squared exact test were subjected to Bonferroni correction. Differences were considered significant at a P-value of <0.05.

Statistical processing and graph drawing were performed using Graph Pad Prism (GraphPad Software Inc., USA). The contingency analysis used the R script [30] to perform the Bonferroni correction.

3. Results

3.1. Effects of cyclic stretching on the distribution of actin and LBs

A549 cells were cultured on a silicone chamber and exposed to equivalent uniaxial strains with a 10 or 20 % change, corresponding to physiological stretching or overstretching, respectively. Fig. 1 shows the time course of representative fluorescence changes. The fluorescent region showed a decreased LB area under no-stretch (Fig. 1A–C) and 10 % stretch (Fig. 1D–F) conditions. In comparison, under the 20 % stretch condition, the LB area size remained unchanged, and the F-actin area increased (Fig. 1G–I). Fig. 2 shows the total LB and F-actin area changes over time in living AE2 cells cultured under no-stretch (Figs. 2A), 10 % stretch (Figs. 2B), and 20 % stretch (Fig. 2C) conditions. Under the no-stretch and 10 % stretch conditions, the F-actin area decreased, while at a 20 % stretch, the F-actin area increased over time. The LB area decreased at 2 h under all stretch conditions; only at a 10 % stretch was the area reduced both at 1 h and 2 h. To compare the LB and F-actin areas among other stretch patterns, we separated the data into LB (Fig. 2D) and F-
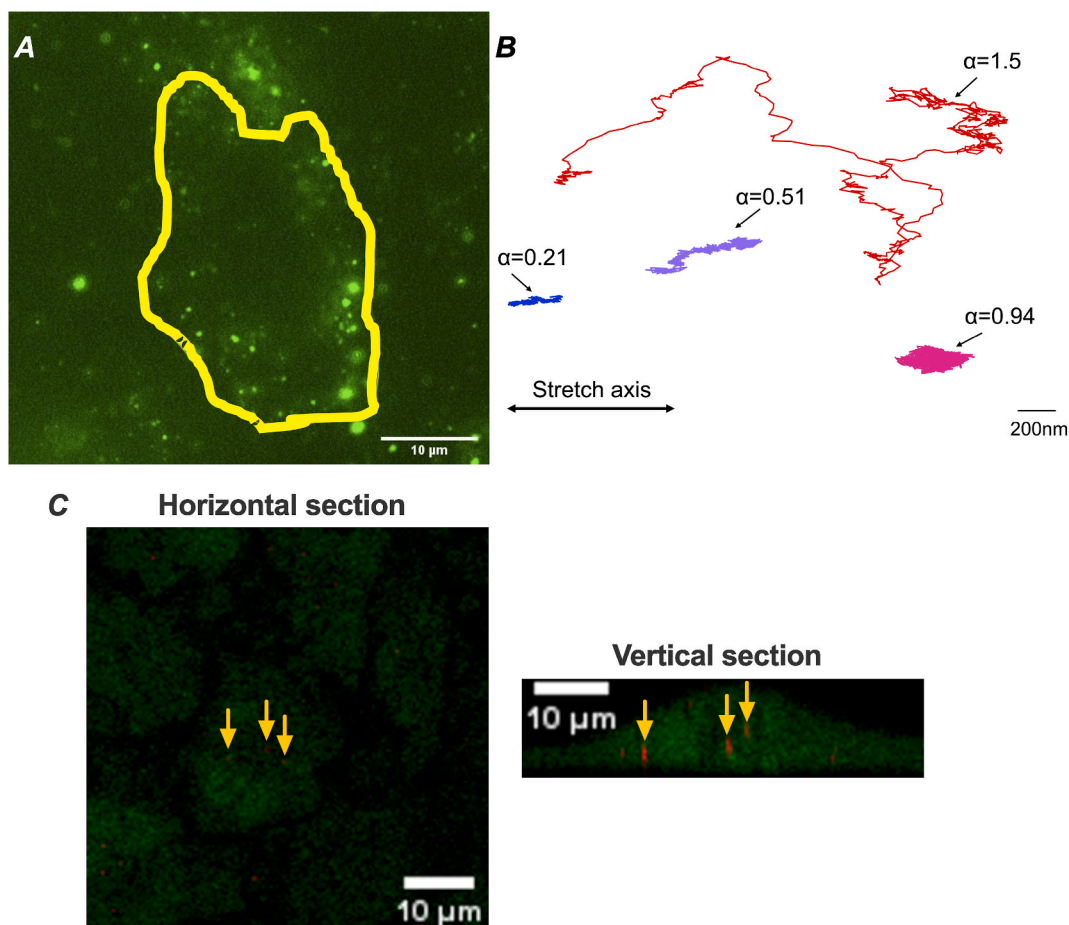
Fig. 4. Representative image of particles introduced into a cell and particle tracking. (A) The representative fluorescence image indicates particles within a living AE2 cell in a silicone chamber. Green particles refer to introduced beads, and thick yellow lines indicate the edges of a cell. (B) The image shows particle tracking for 10 s α is computed from the MSD slope of particle motion at every measurement time in both logarithms and averaged over the observation time. (C) The confocal microscope images of the cells in which the fluorescent particle was introduced. The arrows show the particle location. A549 cells were incubated with 100 nm red polystyrene beads (Carboxylate-Modified Microspheres (Thermo Fisher Scientific)), then CellTracker Green (Thermo Fisher Scientific) was added and stained for 30 min, and the images were observed with a confocal laser microscope. Green indicates intracellular regions and red indicates introduced beads. Scale bars are 10 μm in (A) and (C), and 200 nm in (B). (For interpretation of the references to colour in this figure legend, the reader is referred to the Web version of this article.)

actin (Fig. 2E) data for validation. We found that the LB area had decreased more under the 10 % stretch condition than under either the no-stretch or the 20 % stretch condition at 1 h, whereas the LB area was more prominent in the 20 % stretch than either in the no-stretch or the 10 % stretch at 2 h. Similarly, the F-actin area was significantly larger under the 20 % stretch condition than under other stretch conditions. Thus, overstretching approximately doubled F-actin and suppressed LB secretion by half in fluorescent area ratio compared with physiological stretching.

To elucidate the role of actin polymerization in surfactant secretion from cells, the effects of an actin polymerization inhibitor on LB secretion from A549 cells were analyzed. An inhibitor of actin polymerization, cytochalasin D, increased LB secretion (Supplementary Fig. S1). These results suggest that the overstretching of AE2 cells increases actin polymerization and subsequently suppresses surfactant secretion.
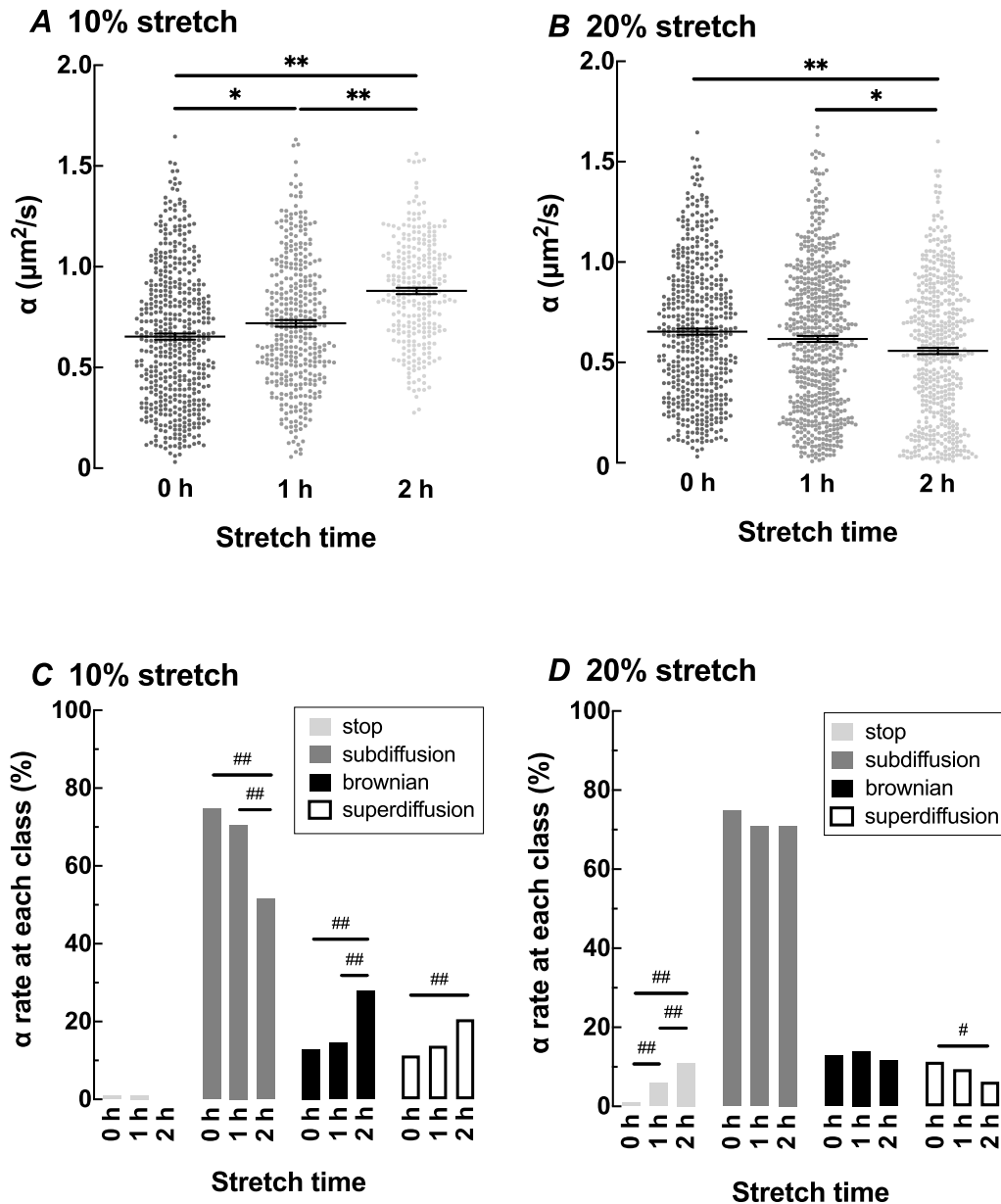
Fig. 5. **Time variation of α.** α with (A) a 10 % stretch (N = 4; 0 h: n = 496; 1 h: n = 370; 2 h: n = 272) and (B) a 20 % stretch (N = 4; 0 h: n = 496; 1 h: n = 596; 2 h: n = 480). The number of silicone chambers and the number of particles are denoted by N and n, respectively. Shown points are individual values. The horizontal black lines are the mean of each data set, and the error bars indicate the standard error of the mean. α values obtained from particle motion are classified as stoppage, subdiffusion, Brownian motion, or superdiffusion. The α at each time course was expressed as a percentage: (C) 10 % stretch; (D) 20 % stretch. *$P < 0.05$, **$P < 0.01$; #$P < 0.05$, ##$P < 0.01$.

To analyze changes to the LB and F-actin area distribution from the bottom to the top of the cell under each stretch condition, we compared the area change in the nine quadrants in the Z-axis of the cells (Fig. 3) based on the area distribution before stretching. Zero in the figures was considered the cell bottom and 8 the cell apex: the smaller the number, the closer to the bottom, and the larger the number, the closer to the top.

The distribution of LBs and the F-actin area under each condition showed a difference over time according to a two-way analysis of
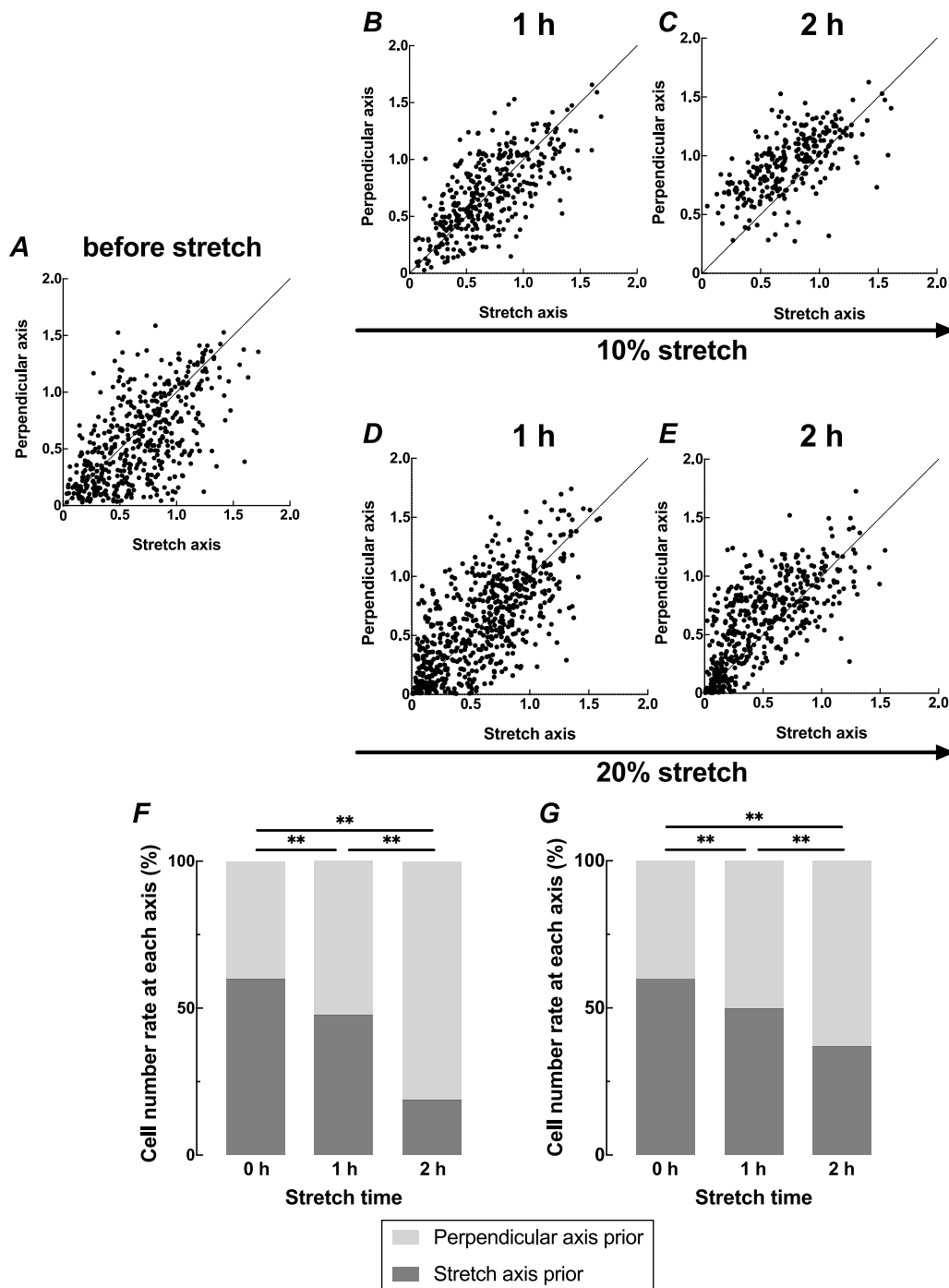
Fig. 6. Time variation of α on the stretch axis and perpendicular axis. Scatter plot of α on each axis in each stretch pattern at each time course: (A) before stretch, (B) 10 % stretch for 1 h, (C) 10 % stretch for 2 h, (D) 20 % stretch for 1 h, and (E) 20 % stretch for 2 h. Shown points are individual values, and the dashed line shows the α identity between the axes. Particles are divided by the axis, which shows a larger α and is summarized as a proportion: (F) 10 % stretch; (G) 20 % stretch. **P < 0.01.

variance (ANOVA) (P < 0.01). However, the plot of the ninth quartile graph indicated that the temporal change in the distribution depended on the stretch conditions. The LB area decreased through the middle of the cells at the 2 h time point under the no-stretch (Fig. 3A, left) and 10 % stretch (Fig. 3B, left) conditions; meanwhile, with a 20 % stretch, an LB area change was observed mainly at the bottom (Fig. 3C, left). Under no-stretch conditions, the F-actin area decreased from the bottom to the center area (Fig. 3A, right), indicating that declining areas in F-actin were observed mainly at the bottom. After a 10 % stretch, the declining F-actin area extended to the upper part of the cells, which was a broader region than under the no-stretch condition (Fig. 3B, right). Surprisingly, under a 20 % stretch condition, the increase in the F-actin area was observed in the upper part of the cells, at points 4 to 8 (Fig. 3C, right).

3.2. Intracellular trafficking changes induced by stretching

It has been shown that the intracellular dynamics of non-functionalized quantum dots depended on the presence of F-actin [18]. Enhanced actin polymerization may contribute to a decrease in intracellular trafficking and also in LB secretion. To evaluate the trafficking, we introduced 100 nm fluorescent particles into cells (Fig. 4A), which we tracked, calculating their MSD and the diffusion exponents (α) that are the slopes of the MSD. Fig. 4B shows the representative trajectories of the particles depending on α. Fig. 4C confirmed that the beads were introduced into the cells. The α index increased gradually under the 10 % stretch condition (Fig. 5A), while under the 20 % stretch condition, the α showed a significant decrease at 2 h (Fig. 5B). Reflecting the increase in α observed at a 10 % stretch (Fig. 5C), there was a decrease in the subdiffusion class and an increase in the percentage of particles in the Brownian motion class and the superdiffusion class. The proportion of particles under a 20 % stretch condition (Fig. 5D) in the stoppage class significantly increased over time; meanwhile, the fractions of particles in the superdiffusion class decreased.

3.3. Changes in actin direction and corresponding intracellular movement

In addition to the magnitude of the particle motion, we also evaluated its direction. The particle motion was divided into the stretch and perpendicular axes, and the α was calculated for each axis (Fig. 6). As a result, the α plot on both axes showed that each point shifted in the upper left direction (Fig. 6 A–E). We classified each particle motion as belonging to the larger numerical value of α on the two axes (stretch axis or perpendicular axis). The proportion of particles in each axis out of the total number of particles was evaluated. To assess the proportion difference between each axis, the chi-squared test was performed and subjected to Bonferroni correction. Both 10 % and 20 % cyclic stretches shifted the α index toward the perpendicular axis (Fig. 6 F–G).

After cyclic stretching, the orientation of F-actin changed significantly, becoming perpendicular to the stretch axis (Supplementary Fig. S2). Particle motion is assumed to be limited in the actin skeleton [18]; therefore, this change in actin orientation would affect the intracellular trafficking.

4. Discussion

The present study demonstrated that the physiological stretching of A549 cells promotes actin fiber depolymerization, induces a higher diffusion index α (facilitates intracellular trafficking), and enhances LB secretion. Meanwhile, extensive invasive stretching to the cells accelerates actin fiber polymerization and reduces the α index (attenuates intracellular trafficking), resulting in LB retention in the cells. An actin polymerization inhibitor increased LB secretion from the cells. These results suggest that the overstretching of AE2 cells increases actin polymerization and decreases intracellular trafficking, leading to the suppression of surfactant secretion. Our results on surfactant secretion, stretch, and actin polymerization in a single cell are consistent with the previous studies in a whole cell population [9,14].

We also analyzed the axis change correlation between the actin direction change and the particle motion direction. Stretching changed the F-actin orientation to perpendicular to the stretch axis, as reported previously with non-living cells [31–33]. Because the F-actin reoriented to the perpendicular axis in both cyclic 10 % and 20 % stretch patterns, the α in the perpendicular direction increased with the expanding space in which the particles were captured in the orthogonal direction in our study. This direction change following actin polymerization also indicates that actin fibers are an important factor in determining intracellular trafficking [18].

By observing identical cells, not the bulk cells population, for the first time, we showed that the physiological stretching of AE2 cells accelerates actin depolymerization and enhances surfactant secretion and that overstretching accelerates actin polymerization and reduces surfactant secretion. These findings are supported by previous studies reporting increased vesicular trafficking to the plasma membrane when cells were subjected to physiological stretch stimuli [9] and stretch-dependent actin polymerization by using single actin filaments and magnetic tweezers *in vitro*. [34] The observed relationship between actin polymerization and intracellular trafficking is in agreement with previous studies, which indicated that F-actin stabilization due to drugs could also reduce intracellular diffusion using COS-7 cells [18].

Under the no-stretch condition, the areas of actin depolymerization were observed mainly at the bottom. This eccentricity is considered to be due to mechanotransduction because it has been reported that actin fibers form according to the stiffnesses of the substrate [35]. Under physiological stretching, actin depolymerization over time was observed, and it spread broadly into the cells. This F-actin distribution change would be explained by actin fiber subtypes, which are classified by intracellular locations [36–38]. Among them, dorsal fibers and transverse fibers, which polymerize from focal adhesions at the leading edge and rise toward the dorsal side of the cell lamella, exist broadly and show a more rapid depolymerization response to a 10 % stretch [31]. This response might reflect our results that the actin fibers decreased widely and rapidly with a 10 % stretch. Meanwhile, with a 20 % stretch, the actin distribution exhibited polymerization in the central to upper areas of the cells. This could be presumed from the previous findings that

the perinuclear cap fibers show slow polymerization responses to mechanical stretching that derive from focal adhesions at the front edge, extend over the nucleus, and culminate in adhesions at the back [31].

The present study showed the association of intracellular trafficking with mechanical stretching. Several studies have shown intracellular rheology and diffusion changes via physical and engineering methods. The cell had viscoelastic properties that reflected both liquids and solids and that changed over time [39]. The MSD revealed heterogeneous and nonergodic motion of microorganisms in the cytosol [40]. An optical tweezer-based method [41,42] showed that intracellular diffusion was associated with intracellular viscoelasticity and dependent on actin polymerization. Finally, a phase-sensitive acoustic microscope was used to evaluate the viscoelasticity of gels containing actin, determining that the actin polymerization rate was proportional to the viscosity [43]. With these studies, mechanism of excessive actin polymerization expected to impair secretion both by steric hindrance to the movement of organelles such as LBs and by a general change into the viscoelastic properties of the cytosol. Our study showed the motion change toward actin polymerization direction in Fig. 6, actin filament was considered to mainly be a physical obstruction to secretion.

This study had some limitations. We used A549 cells as AE2 cells. A549 cells have been widely applied in past studies [17,22,44], but A549 cells are continuous tumor-cell lines from a human lung carcinoma cancer cell, which would not fully reflect physiological changes. In a real lung environment, the epithelium consists of various cell types, particularly ATII and ATI cells, which would be the ones suffering most of the overstretching stimulus. We need further study to understand what extent ATII cells would sense and respond to the mechanical stress under that more complex scenario. Second, we observed that the secretion change was distinct from the quinacrine fluorescent area change. Quinacrine was incorporated into surfactant micelles [45] and used as LB staining [17,20], accumulated mainly in the acidic lamellar bodies on AE2 cells [19]. Third, to directly observe vesicular transport, proteins related to vesicular transport, such as Rab proteins [46] or P2X4 receptor proteins [20], are expected to be used. The quinacrine-stained vesicles used in the present study were shown to be transported the same as these substances. For evaluating intracellular trafficking, 100 nm diameter fluorescent particles were used. Research evaluating the MSD of A549 cells pointed out that the motion of the same particle size in the vesicle was not dependent on the size from 50 nm diameter to 300 nm [47]. Our aim was to investigate possible changes in intracellular transport among stretch conditions. The size of particles used in the present study did not deviate from the aforementioned range. We used particles of the same radius among the conditions. Therefore, we considered that the results would be unlikely to be affected. Finally, surfactant delivery to the air–liquid interface in the lung depends on its synthesis and secretion from AE2 cells [2]. We did not evaluate the effects of invasive cyclic stretching on surfactant synthesis in this study.

Our studies provide evidence that stretching AE2 cells alters actin fiber polymerization and intracellular trafficking, consequently affecting surfactant secretion. A pulmonary surfactant reduces surface tension in the alveoli, preventing collapse during expiration and facilitating re-expansion during inspiration. Surfactants also play crucial roles in innate defense and immune regulation in the lungs. We believe the results of this study will provide valuable insights into surfactant delivery to the alveolar surface and critical alterations to cellular physiology due to mechanical stretch loading.

Funding information

Ethics approval and consent to participate

Not applicable.

Data availability statement

The data associated with this study has not been deposited into a publicly available repository. Data will be made available on request.

CRediT authorship contribution statement

Shigesato Inoue: Writing – original draft, Visualization, Validation, Software, Investigation, Formal analysis, Data curation, Conceptualization. **Junpei Nagao:** Software, Methodology, Investigation, Formal analysis. **Kouhei Kawamoto:** Software, Methodology, Investigation, Formal analysis. **Keiko Kan-o:** Writing – review & editing. **Satoru Fukuyama:** Writing – review & editing, Funding acquisition. **Saori Sasaki:** Data curation. **Susumu Kudo:** Writing – review & editing, Supervision, Funding acquisition, Conceptualization. **Isamu Okamoto:** Writing – review & editing. **Toshihiro Sera:** Writing – review & editing, Supervision, Resources, Project administration, Funding acquisition, Conceptualization.

Declaration of competing interest

The authors declare that they have no known competing financial interests or personal relationships that could have appeared to influence the work reported in this paper.

Acknowledgments

Appendix A. Supplementary data

Supplementary data to this article can be found online at https://doi.org/10.1016/j.heliyon.2024.e33499.

References

[1] E. Lopez-Rodriguez, J. Pérez-Gil, Structure-function relationships in pulmonary surfactant membranes: from biophysics to therapy, Biochim. Biophys. Acta 1838 (2014) 1568–1585, https://doi.org/10.1016/j.bbamem.2014.01.028.
[2] A.V. Andreeva, M.A. Kutuzov, T.A. Voyno-Yasenetskaya, Regulation of surfactant secretion in alveolar type II cells, Am. J. Physiol. Lung Cell Mol. Physiol. 293 (2007), https://doi.org/10.1152/ajplung.00112.2007.
[3] B. Ruaro, P. Confalonieri, R. Pozzan, S. Tavano, L. Mondini, E. Baratella, A. Pagnin, S. Lerda, P. Geri, M. Biolo, et al., Severe COVID-19 ARDS treated by bronchoalveolar lavage with diluted exogenous pulmonary surfactant as salvage therapy: in pursuit of the holy grail? JCM 11 (2022) 3577, https://doi.org/10.3390/jcm11133577.
[4] A. Dushianthan, M.P.W. Grocott, G.S. Murugan, T.M.A. Wilkinson, A.D. Postle, Pulmonary surfactant in adult ARDS: current perspectives and future directions, Diagnostics 13 (2023) 2964, https://doi.org/10.3390/diagnostics13182964.
[5] S. Buckingham, M.E. Avery, Time of appearance of lung surfactant in the foetal mouse, Nature 193 (1962) 688–689, https://doi.org/10.1038/193688a0.
[6] H.R. Wirtz, L.G. Dobbs, Calcium mobilization and exocytosis after one mechanical stretch of lung epithelial cells, Science 250 (1990) 1266–1269, https://doi.org/10.1126/science.2173861.
[7] C.M. Waters, E. Roan, D. Navajas, Mechanobiology in lung epithelial cells: measurements, perturbations, and responses, Compr. Physiol. 2 (2012) 1–29, https://doi.org/10.1002/cphy.c100090.
[8] R.K. Albert, Constant V t ventilation and surfactant dysfunction: an overlooked cause of ventilator-induced lung injury, Am. J. Respir. Crit. Care Med. 205 (2022) 152–160, https://doi.org/10.1164/rccm.202107-1690CP.
[9] S.P. Arold, E. Bartolák-Suki, B. Suki, Variable stretch pattern enhances surfactant secretion in alveolar type II cells in culture, Am. J. Physiol. Lung Cell Mol. Physiol. 296 (2009) L574–L581, https://doi.org/10.1152/ajplung.90454.2008.
[10] P. Li, A.T. Bademosi, J. Luo, F.A. Meunier, Actin remodeling in regulated exocytosis: toward a mesoscopic view, Trends Cell Biol. 28 (2018) 685–697, https://doi.org/10.1016/j.tcb.2018.04.004.
[11] P. Miklavc, E. Hecht, N. Hobi, O.H. Wittekindt, P. Dietl, C. Kranz, M. Frick, Actin coating and compression of fused secretory vesicles are essential for surfactant secretion – a role for Rho, formins and myosin II, J. Cell Sci. 125 (2012) 2765–2774, https://doi.org/10.1242/jcs.105262.
[12] P. Miklavc, O.H. Wittekindt, E. Felder, P. Dietl, Ca2+-dependent actin coating of lamellar bodies after exocytotic fusion: a prerequisite for content release or kiss-and-run, Ann. N. Y. Acad. Sci. 1152 (2009) 43–52, https://doi.org/10.1111/j.1749-6632.2008.03989.x.
[13] T.K. Singh, B. Abonyo, T.A. Narasaraju, L. Liu, Reorganization of cytoskeleton during surfactant secretion in lung type II cells: a role of annexin II, Cell. Signal. 16 (2004) 63–70, https://doi.org/10.1016/s0898-6568(03)00089-5.
[14] F. Rose, C. Kürth-Landwehr, U. Sibelius, K.H. Reuner, K. Aktories, W. Seeger, F. Grimminger, Role of actin depolymerization in the surfactant secretory response of alveolar epithelial type II cells, Am. J. Respir. Crit. Care Med. 159 (1999) 206–212, https://doi.org/10.1164/ajrccm.159.1.9801106.
[15] G. Eitzen, Actin remodeling to facilitate membrane fusion, Biochim. Biophys. Acta Mol. Cell Res. 1641 (2003) 175–181, https://doi.org/10.1016/S0167-4889(03)00087-9.
[16] J. Stricker, T. Falzone, M.L. Gardel, Mechanics of the F-actin cytoskeleton, J. Biomech. 43 (2010) 9–14, https://doi.org/10.1016/j.jbiomech.2009.09.003.
[17] S.K. Mahto, J. Tenenbaum-Katan, A. Greenblum, B. Rothen-Rutishauser, J. Sznitman, Microfluidic shear stress-regulated surfactant secretion in alveolar epithelial type II cells in vitro, Am. J. Physiol. Lung Cell Mol. Physiol. 306 (2014) L672–L683, https://doi.org/10.1152/ajplung.00106.2013.
[18] E.A. Katrukha, M. Mikhaylova, H.X. van Brakel, P.M. van Bergen en Henegouwen, A. Akhmanova, C.C. Hoogenraad, L.C. Kapitein, Probing cytoskeletal modulation of passive and active intracellular dynamics using nanobody-functionalized quantum dots, Nat. Commun. 8 (2017) 14772, https://doi.org/10.1038/ncomms14772.
[19] N.R. Chintagari, A. Mishra, L. Su, Y. Wang, S. Ayalew, S.D. Hartson, L. Liu, Vacuolar ATPase regulates surfactant secretion in rat alveolar type II cells by modulating lamellar body calcium, PLoS One 5 (2010) e9228, https://doi.org/10.1371/journal.pone.0009228.
[20] G. Fois, V.E. Winkelmann, L. Bareis, L. Staudenmaier, E. Hecht, C. Ziller, K. Ehinger, J. Schymeinsky, C. Kranz, M. Frick, ATP is stored in lamellar bodies to activate vesicular P2X4 in an autocrine fashion upon exocytosis, J. Gen. Physiol. 150 (2018) 277–291, https://doi.org/10.1085/jgp.201711870.
[21] G. Lukinavičius, L. Reymond, E. D'Este, A. Masharina, F. Göttfert, H. Ta, A. Güther, M. Fournier, S. Rizzo, H. Waldmann, et al., Fluorogenic probes for live-cell imaging of the cytoskeleton, Nat. Methods 11 (2014) 731–733, https://doi.org/10.1038/nmeth.2972.
[22] Y. Ren, Q. Zhan, Q. Hu, B. Sun, C. Yang, C. Wang, Static stretch induces active morphological remodeling and functional impairment of alveolar epithelial cells, Respiration 78 (2009) 301–311, https://doi.org/10.1159/000207632.
[23] V. Briane, C. Kervrann, M. Vimond, Statistical analysis of particle trajectories in living cells, Phys. Rev. 97 (2018), https://doi.org/10.1103/PhysRevE.97.062121.
[24] C.A. Schneider, W.S. Rasband, K.W. Eliceiri, NIH Image to ImageJ: 25 years of image analysis, Nat. Methods 9 (2012), https://doi.org/10.1038/nmeth.2089.
[25] J.Y. Tinevez, N. Perry, J. Schindelin, G.M. Hoopes, G.D. Reynolds, E. Laplantine, S.Y. Bednarek, S.L. Shorte, K.W. Eliceiri, TrackMate: an open and extensible platform for single-particle tracking, Methods 115 (2017), https://doi.org/10.1016/j.ymeth.2016.09.016.
[26] H. Qian, M.P. Sheetz, E.L. Elson, Single particle tracking. Analysis of diffusion and flow in two-dimensional systems, Biophys. J. 60 (1991), https://doi.org/10.1016/S0006-3495(91)82125-7.
[27] X. Michalet, Mean square displacement analysis of single-particle trajectories with localization error: Brownian motion in an isotropic medium, Phys. Rev. E - Stat. Nonlinear Soft Matter Phys. 82 (2010), https://doi.org/10.1103/PhysRevE.82.041914.
[28] F. Huang, E. Watson, C. Dempsey, J. Suh, Real-time particle tracking for studying intracellular trafficking of pharmaceutical nanocarriers, in: V. Weissig, T. Elbayoumi, M. Olsen (Eds.), Cellular and Subcellular Nanotechnology Methods in Molecular Biology, Humana Press, 2013, pp. 211–223, https://doi.org/10.1007/978-1-62703-336-7_20.
[29] V. Briane, M. Vimond, C. Kervrann, An overview of diffusion models for intracellular dynamics analysis, Briefings Bioinf. 21 (2019), https://doi.org/10.1093/bib/bbz052.
[30] R Core Team, R: A Language and Environment for Statistical Computing, 2021.
[31] A. Roshanzadeh, T.T. Nguyen, K.D. Nguyen, D.-S. Kim, B.-K. Lee, D.-W. Lee, E.-S. Kim, Mechanoadaptive organization of stress fiber subtypes in epithelial cells under cyclic stretches and stretch release, Sci. Rep. 10 (2020) 18684, https://doi.org/10.1038/s41598-020-75791-2.

[32] A.M. Greiner, H. Chen, J.P. Spatz, R. Kemkemer, Cyclic tensile strain controls cell shape and directs actin stress fiber formation and focal adhesion alignment in spreading cells, PLoS One 8 (2013) e77328, https://doi.org/10.1371/journal.pone.0077328.

[33] K. Nagayama, T. Fukuei, Cyclic stretch-induced mechanical stress to the cell nucleus inhibits ultraviolet radiation-induced DNA damage, Biomech. Model. Mechanobiol. 19 (2020), https://doi.org/10.1007/s10237-019-01224-3.

[34] M. Yu, X. Yuan, C. Lu, S. Le, R. Kawamura, A.K. Efremov, Z. Zhao, M.M. Kozlov, M. Sheetz, A. Bershadsky, et al., mDia1 senses both force and torque during F-actin filament polymerization, Nat. Commun. 8 (2017) 1650, https://doi.org/10.1038/s41467-017-01745-4.

[35] S. Asano, S. Ito, K. Takahashi, K. Furuya, M. Kondo, M. Sokabe, Y. Hasegawa, Matrix stiffness regulates migration of human lung fibroblasts, Physiol Rep 5 (2017) e13281, https://doi.org/10.14814/phy2.13281.

[36] M. Maninová, T. Vomastek, Dorsal stress fibers, transverse actin arcs, and perinuclear actin fibers form an interconnected network that induces nuclear movement in polarizing fibroblasts, FEBS J. 283 (2016) 3676–3693, https://doi.org/10.1111/febs.13836.

[37] S.B. Khatau, C.M. Hale, P.J. Stewart-Hutchinson, M.S. Patel, C.L. Stewart, P.C. Searson, D. Hodzic, D. Wirtz, A perinuclear actin cap regulates nuclear shape, Proc. Natl. Acad. Sci. U. S. A. 106 (2009) 19017–19022, https://doi.org/10.1073/pnas.0908686106.

[38] D.H. Kim, S.B. Khatau, Y. Feng, S. Walcott, S.X. Sun, G.D. Longmore, D. Wirtz, Actin cap associated focal adhesions and their distinct role in cellular mechanosensing, Sci. Rep. 2 (2012), https://doi.org/10.1038/srep00555.

[39] K.E. Kasza, A.C. Rowat, J. Liu, T.E. Angelini, C.P. Brangwynne, G.H. Koenderink, D.A. Weitz, The cell as a material, Curr. Opin. Cell Biol. 19 (2007) 101–107, https://doi.org/10.1016/j.ceb.2006.12.002.

[40] C. Åberg, B. Poolman, Glass-like characteristics of intracellular motion in human cells, Biophys. J. 120 (2021) 2355–2366, https://doi.org/10.1016/j.bpj.2021.04.011.

[41] H.C. Yalcin, K.M. Hallow, J. Wang, M.T. Wei, H.D. Ou-Yang, S.N. Ghadiali, Influence of cytoskeletal structure and mechanics on epithelial cell injury during cyclic airway reopening, Am. J. Physiol. Lung Cell Mol. Physiol. 297 (2009) L881–L891, https://doi.org/10.1152/ajplung.90562.2008.

[42] K. Mandal, A. Asnacios, B. Goud, J.-B. Manneville, Mapping intracellular mechanics on micropatterned substrates, Proc. Natl. Acad. Sci. U.S.A. 113 (2016), https://doi.org/10.1073/pnas.1605112113.

[43] O. Wagner, J. Zinke, P. Dancker, W. Grill, J. Bereiter-Hahn, Viscoelastic properties of f-actin, microtubules, f-actin/_-actinin, and f-actin/Hexokinase determined in microliter volumes with a novel nondestructive method, Biophys. J. 76 (1999).

[44] N.E. Vlahakis, M.A. Schroeder, A.H. Limper, R.D. Hubmayr, Stretch induces cytokine release by alveolar epithelial cells in vitro, Am. J. Physiol. Lung Cell Mol. Physiol. 277 (1999) L167–L173, https://doi.org/10.1152/ajplung.1999.277.1.L167.

[45] M. Usman, M. Siddiq, Probing the micellar properties of Quinacrine 2HCl and its binding with surfactants and human serum albumin, Spectrochim. Acta Mol. Biomol. Spectrosc. 113 (2013) 182–190, https://doi.org/10.1016/j.saa.2013.04.089.

[46] F. Marceau, M.-T. Bawolak, J. Bouthillier, G. Morissette, Vacuolar ATPase-mediated cellular concentration and retention of quinacrine: a model for the distribution of lipophilic cationic drugs to autophagic vacuoles, Drug Metab. Dispos. 37 (2009) 2271–2274, https://doi.org/10.1124/dmd.109.028480.

[47] M. Aoyama, M. Yoshioka, Y. Arai, H. Hirai, R. Ishimoto, K. Nagano, K. Higashisaka, T. Nagai, Y. Tsutsumi, Intracellular trafficking of particles inside endosomal vesicles is regulated by particle size, J. Contr. Release 260 (2017) 183–193, https://doi.org/10.1016/j.jconrel.2017.06.007.